

\mathcal{R}^2 -CNN: Fast Tiny Object Detection in Large-scale Remote Sensing Images

Jiangmiao Pang , Cong Li , Jianping Shi , Zhihai Xu, Huajun Feng

Abstract—Recently, convolutional neural network has brought impressive improvements for object detection. However, detecting tiny objects in large-scale remote sensing images still remains challenging. Firstly, the extreme large input size makes existing object detection solutions too slow for practical use. Secondly, the massive and complex backgrounds cause serious false alarms. Moreover, the ultra tiny objects increase the difficulty of accurate detection. To tackle these problems, we propose a unified and self-reinforced network called \mathcal{R}^2 -CNN: Remote sensing Region-based Convolutional Neural Network, composing of backbone Tiny-Net, intermediate global attention block, and final classifier and detector. Tiny-Net is a lightweight residual structure which enables fast and powerful features extraction from inputs. Global attention block is built upon Tiny-Net to inhibit false positives. Classifier is then used to predict the existence of target in each patch, and detector is followed to locate them accurately if available. The classifier and detector are mutually reinforced with end-to-end training, which further speed-up the process and avoid false alarms. Effectiveness of \mathcal{R}^2 -CNN is validated on hundreds of GF-1 images and GF-2 images, which are 18000×18192 pixels, 2.0m resolution, and 27620×29200 pixels, 0.8m resolution respectively. Specifically, we can process a GF-1 image in 29.4s on Titian X just with single thread. According to our knowledge, no previous solution can detect tiny object on such huge remote sensing images gracefully. We believe that it is a significant step towards practical real-time remote sensing systems.

Index Terms—Object detection, Remote Sensing Images, Remote sensing Region-based Convolutional Neural Network(\mathcal{R}^2 -CNN)

I. INTRODUCTION

THANKS to the development of optical remote sensing imaging technology, high-resolution images can be easily obtained, which help us understand the earth better. Object detection, change detection, semantic segmentation and other tasks become popular in remote sensing area.

[1]–[5] propose different approaches for object detection in remote sensing images with the powerful feature extraction capability of deep convolutional neural networks. But those methods are mainly focus on small region segments comparing to the original large inputs, e.g., usually over than 20000×20000 pixels. Therefore they can not scale up to handle such huge images gracefully. Zhang et al. [4] attempted to detect airports at first to speed-up the process in large-scale images, but the training and testing images are all from

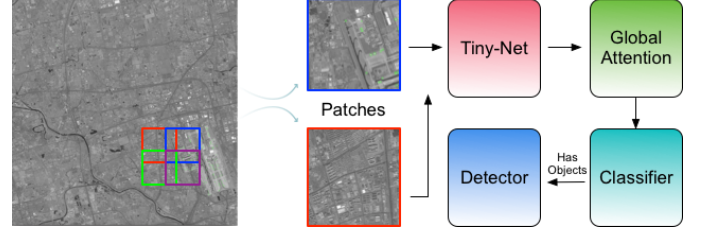


Fig. 1: \mathcal{R}^2 -CNN is a unified network working in patch-wise manner. Pipeline is shown on the right.

regions near to airports, which escaping from the complex backgrounds. According to our experiments, it is not robust enough for practical applications.

Object detection in large-scale remote sensing images is pretty challenging. Firstly, the scale of input image is too large to reach practical application. The computation time and memory consumption are increased quadratically, making it too slow and not runnable on current hardware. Secondly, massive and complex backgrounds appear in real scenario may introduce more false positives. For instance, desert region with random texture, or urban area with massive building structure, etc. Moreover, the performance drops drastically with tiny objects (such as 8-32 pixels), especially in low-resolution images, which further increases the difficulty of tiny object detection in remote sensing images.

To tackle these problems, we propose a unified and self-reinforced convolutional neural network called \mathcal{R}^2 -CNN: Remote sensing Region-based Convolutional Neural Network, which is composed of backbone Tiny-Net, intermediate global attention block, and the final classifier and detector, enable the entire network *efficient* in both computation and memory consumption, *robust* to false positives and *strong* to detect tiny objects. Pipeline is shown in Fig 1.

Firstly, as a unified and self-reinforced framework, \mathcal{R}^2 -CNN first crops large scale images with a much more smaller scale (such as 640×640 pixels) with 20% overlap to tackle the oversized input size. By processing the patches asynchronously, the limited memory is not a problem anymore. A convolutional backbone structure is then applied to inputs which enables powerful features extraction. Based on the discriminative features, the classifier first predict the existence of detection target in current patch, and a detector is followed to locate them accurately if available. The classifier and detector are mutually reinforced each other under the end-to-end training framework. There are two advantages of this self-reinforced architecture:

This work is supported by Basic Research ID JCKY2018110C081. Corresponding author is Huajun Feng.

J. Pang, Z. Xu, H. Feng are with Zhejiang University, Hangzhou, China. E-mails: pjim@zju.edu.cn, xuzh@zju.edu.cn, fenghj@zju.edu.cn.

C. Li and J. Shi are with SenseTime Research, Beijing, China. E-mails: licong@sensetime.com, shijianping@sensetime.com.

- 1) Since in large-scale remote sensing images most crops do not contain valid target, so that about 99% of the total patches do not need to pass the heavy detector branch. The light classifier branch can filter out blank patch without more heavy detector cost.
- 2) As most false positives commonly occurs with massive backgrounds, benefit from the self-reinforced framework, the classifier can identify the difficult situation even when there is only one tiny objects in the patch given the fine-grained features from detector. On the other hand, detector receives less false positive candidates since most of them are filtered out by classifier. Even if the patches are distinguished incorrectly by classifier, the detector can still rectify the results later.

Secondly, we specially designed a lightweight residual network called Tiny-Net, to reduce the inference cost and preserve powerful features for object detection. Tiny-Net is motivated by [6] but is much more lightweight. On the other hand, Tiny-Net can be trained from scratch with a cycle training schedule because of the much less parameters, making the framework do not be influenced by the limited training samplers and the domain gap between natural images and remote sensing images.

Thirdly, to further inhibit the false positives, we also use feature pyramid pooling as a global attention block on the top of Tiny-Net. The feature maps are firstly pooled in different pyramid levels, such as 1×1 , 2×2 , and 4×4 . Then we recover the pooled features to their original scale with bilinear interpolation. The feature maps are fused additionally next. Feature maps get more context information, and the receptive field is also enlarged to the whole image. The detector is more discriminative with the help of more context information. We can found the confidence of false positives drop obviously with this module, proving its effectiveness.

Finally, to make the framework strong to detect tiny objects, we comprehensively analyze why the detected performance drop drastically with tiny objects, and proposed a scale-invariant anchor strategy to tile anchors reasonably especially for small objects based on the region proposal network in [7] framework. On the other hand, we insert an efficient zoom-out and zoom-in architecture in Tiny-Net to enlarge the feature maps, which improve the recall of tiny objects obviously. Position sensitive RoI pooling [8] is also used to share the computation from all detector on the entire image and get more spatial information, which is faster and more accurate than original RoI pooling in [7].

Our contributions can be summarized into four components:

- 1) We proposed a unified and self-reinforced framework called \mathcal{R}^2 -CNN, which is *efficient* in computation and memory consumption, *robust* to false positives and *strong* to detect tiny objects.
- 2) We proposed Tiny-Net, a lightweight residual network which can be trained from scratch and further improve the efficiency.
- 3) We insert a global attention block into \mathcal{R}^2 -CNN to further inhibit the false positives.
- 4) We comprehensively analyze why the detected performance drop drastically with tiny objects and then make

the framework strong to detect tiny objects.

The remainder of this paper is organized as follows. In section II, we briefly introduce state-of-art object detection methods and their applications on remote sensing systems. Then we explain the details of our \mathcal{R}^2 -CNN in section III, and show experiments in section IV. Finally, section V concludes this paper with a discussion of the results.

II. RELATED WORK

As a fundamental problem in remote sensing area, object detection in remote sensing images has been extensively studied in recent years. Previous methods (such as SIFT [9] and HoG [10] [11], etc) use low-level or middle-level feature representations to detect objects. Recently, impressive improvements have achieved with convolutional neural networks. Cheng et al. [12] provide a review of the recent progress in those fields and propose two promising research directions, which are deep learning based methods and weakly supervised learning based methods.

Convolutional neural networks got start from LeNet [13] and became popular with AlexNet [14]. Many impressive methods are proposed to promote the development of image recognition from then on, such as Network-in-Network [15], VGGNet [16] and GoogLeNet [17]. ResNet [6] is a milestone which using residual connections to train very deep convolutional models. It made a great improvement in image recognition. Object detectors like OverFeat [18] and R-CNN [19] made dramatic improvements in accuracy with those deep learning based feature representations. OverFeat adopted a Conv-Net as a sliding window detector on an image pyramid. R-CNN adopted a region proposal-based method based on Selective Search [20], and then use a Conv-Net to classify the scale-normalized proposals. SPP [21] adopted R-CNN on feature maps extracted on a single image scale, which demonstrated that such region-based detectors could be applied much more efficiently. Fast R-CNN [22] and Faster R-CNN [7] made a unified object detector in a multi-task manner. Region proposal networks are proposed to replace Selective Search. Dai, et, al. [8] proposed R-FCN, which use position-sensitive RoI pooling to get a faster and better detector. While those region-based methods are too slow for practical use, single stage detector (such as YOLO [23] and SSD [24]) are proposed to accelerate the processing speed but with a performance drop, especially in small objects.

Along with the rapid development with those mechanisms, small object detection seems much more difficulty thus researchers proposed many frameworks for small object detection specifically. Those methods mainly focus on how to implement a multi-scale framework elegantly or using hard mining method which let the network pay more attention to small objects. Lin et al. proposed feature pyramid networks [25] which uses top-down architecture with lateral connections as an elegant multi-scale feature warping method. Zhang et al. proposed [26] which proposed a scale-equitable face detection framework to handle different scales of faces well. [27] shows that context is crucial and defines templates that make use of massively-large receptive fields. [28] proposed a pyramid

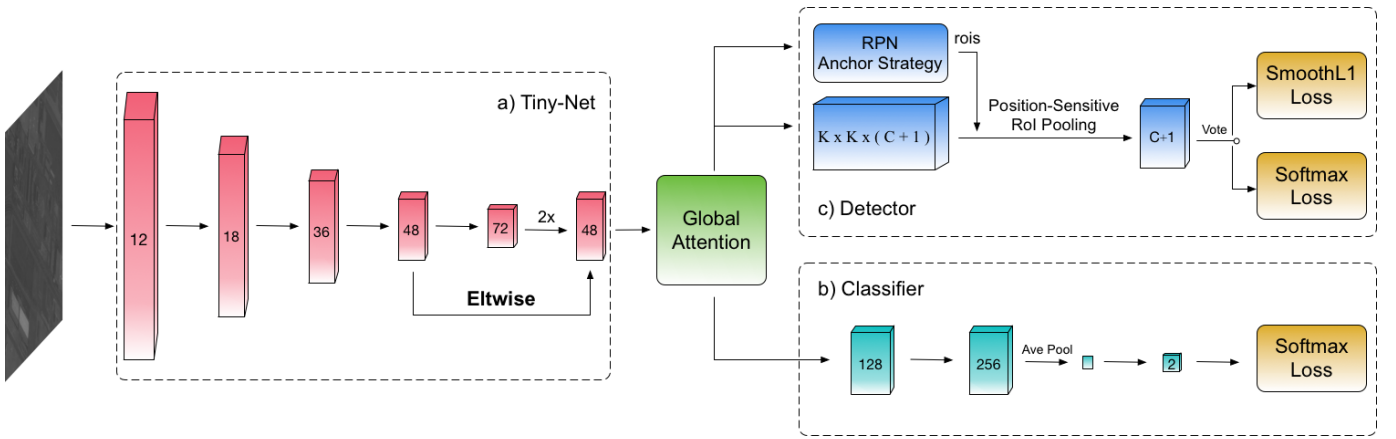


Fig. 2: The architecture of our \mathcal{R}^2 -CNN. a) Tiny-Net, a lightweight residual structure which enables fast and powerful features extraction from inputs. b) Classifier, which can speed-up the unified network and avoid false alarm raised by massive backgrounds. c) Detector, which can locate target objects accurately if available. The classifier and detector are mutually reinforced each other under the end-to-end training framework. In addition, global attention block is built on top of Tiny-Net to inhibit false positives.

scene parsing network which employ the context reasonable. [29] proposed an online hard example mining method which can improve the performance of small objects obviously.

Many methods [1]–[5], [30]–[35] are proposed to improve the object detection accuracy in remote sensing images with convolutional neural networks. Those methods often use pre-trained CNN models on large datasets to handle the limited remote sensing training data. Zhang et al. [31] used trained CNN models to extract surrounding features. Those features were combined with features from HoG to get final representations, and then applied gradient orientation to generate region proposals. Zhu et al. [36] used CNN features from multi-level layers for object detection, which handle the scale-invariance with single scale input. Jiang et al. [37] used a graph-based super-pixel segmentation to generate proposals and then trained a CNN to classify these proposals into different classes. Cheng et al. [35] introduced a rotation-invariant operator to existing CNN architectures and achieves significantly performance. Long, et al. [2] proposed an unsupervised score-based bounding box regression for accurate object localization in remote sensing images. Those methods mainly focus small region segment compared to the original large remote sensing image input, usually over 10000×10000 pixels, thus they cannot scale-up to handle such large input gracefully. Zhang et al. [4] attempted to detect airports in large-scale images first to reduce overall airplane detection time, but the training and testing images are all from region near airports without arbitrary massive backgrounds. For practical use, object detection in large-scale remote sensing images is very important and necessary.

III. PROPOSED METHOD

The \mathcal{R}^2 -CNN, shown in Fig 2, consists of backbone Tiny-Net, intermediate global attention block, and the final classifier and detector.

A. \mathcal{R}^2 -CNN

\mathcal{R}^2 -CNN is a unified and self-reinforced framework working in end-to-end manner. Considering the large input image size increases the computation time and memory consumption quadratically, large-scale remote sensing images (such as 20000×20000 pixels) are cropped with a much more smaller scale (such as 640×640 pixels) with 20% overlap. By processing the patches asynchronously, the limited memory is not a problem anymore.

A convolutional backbone structure is then applied to inputs which enables powerful features extraction. Based on those discriminative features, the classifier first predict the existence of detection target in current patch, and a detector is followed to locate them accurately if available. The classifier and detector are mutually reinforced each other under the end-to-end training framework. There are two advantages of this self-reinforced architecture:

Firstly, the light classifier branch can filter out blank patch without more heavy detector cost. Classifier's architecture is in Fig 2-b), we just use two CONV-BN-RELU blocks to extract features from the former features. Global average pooling and a 1×1 convolutional operator are then attached to it. Softmax loss is employed to guide the training of classifier. Considering most crops do not contain valid target in remote sensing images, about 99% of the total patches do not need to pass the heavy detector branch.

Secondly, massive and complex backgrounds appear in real scenario may introduce more false positive, for instance, desert region with random texture, or urban area with massive building structure, etc. The false positives are firstly inhibited by the mutually reinforcement from the classifier and the detector. Classifier can distinguish the difficult situation even when there is only one tiny objects (such as 12×12 pixels) in the patch. We explain this promotion mainly given the fine-grained feature extracted from detector. On the other hand, detector receives less false positive candidates since most of

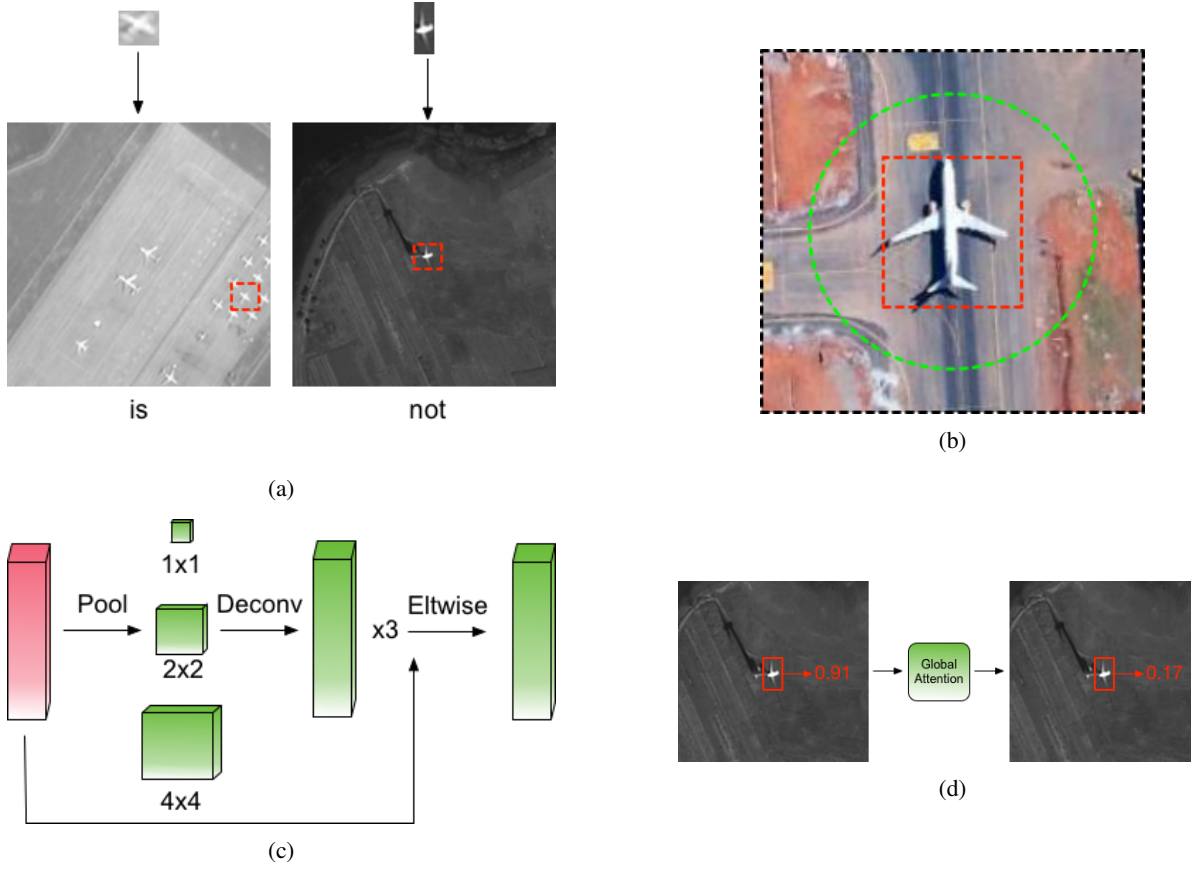


Fig. 3: (a) Whether they are airplane or not? (b) Black: theoretical receptive field. Green: effective receptive field. Red: bounding box. (c) Global attention block. (d) False positive's confidence drop obviously with global attention.

them are filtered out by classifier. Even if the patches are distinguished incorrectly by classifier, the detector can still rectify the results later.

There are three outputs from our network. One output m from classifier represents the probability of whether there are target objects in corresponding patch or not. Two outputs from detector represent the discrete probability ($p = (p_0, \dots, p_k)$) distribution of each RoI over $K + 1$ categories, and bounding-box regression offsets, $t^k = (t_x^k, t_y^k, t_w^k, t_h^k)$, for each of the K object classes, index by k , in corresponding patch. We use the parameterization for t^k in [19], in which t^k represents a scale-invariant translation and log-space height/width shift relative to an object proposal. Each training patches is labeled with a binary ground-truth n , and each RoI in detector is labeled with a ground-truth class u and a ground-truth bounding-box regression target v . We use a unified multi-task loss L on each patch to joint classifier and detector:

$$L(m, n, p, u, t^u, v) = L_{cls}(m, n) + \mu[n = 1](L_{cls}(p, u) + \lambda[u \geq 1]L_{loc}(t^u, v)), \quad (1)$$

in which $L_{cls}(p, u)$ and $L_{cls}(m, n)$ are softmax loss and L_{loc} is smooth-L1 Loss in [7]. The hyper-parameter λ and μ in Eq.1 controls the balance between the three task losses. All experiment use $\lambda = 1$ and $\mu = 1$. We only back-propagate detector's loss when there are detection targets in

corresponding patch during training time. The entire network is *efficient*, *robust*, and *strong*.

B. Tiny-Net

Recently, CNN based methods often use VGG [16] or ResNets [6] as feature extractors. Those models are pre-trained on ImageNet [38], a large-scale hierarchical image database with millions of images, to deal with the limited training samples and get a much more quicker convergence. But there are still many disadvantages when using those pre-trained models. Firstly, those models are too heavy to reach real-time efficiency. Secondly, those models are designed specifically for image classification, make the feature resolution may be not enough for object detection. Finally, considering the heavy parameters, training scratch is pretty difficult especially with limited training samplers. When apply the pre-trained models to remote sensing frameworks, the domain gap between natural images and remote sensing images may make the models sub-optimal.

The architecture of Tiny-Net is shown in Table I. The 3×3 block is residual block in ResNet [6] except conv-1. We do not apply the downsample operator in conv-1 to enable the feature maps more discriminative for tiny object detection, which is different from ImageNet pre-train models such as VGG [16] and ResNets [6]. The parameters of Tiny-Net are far less than

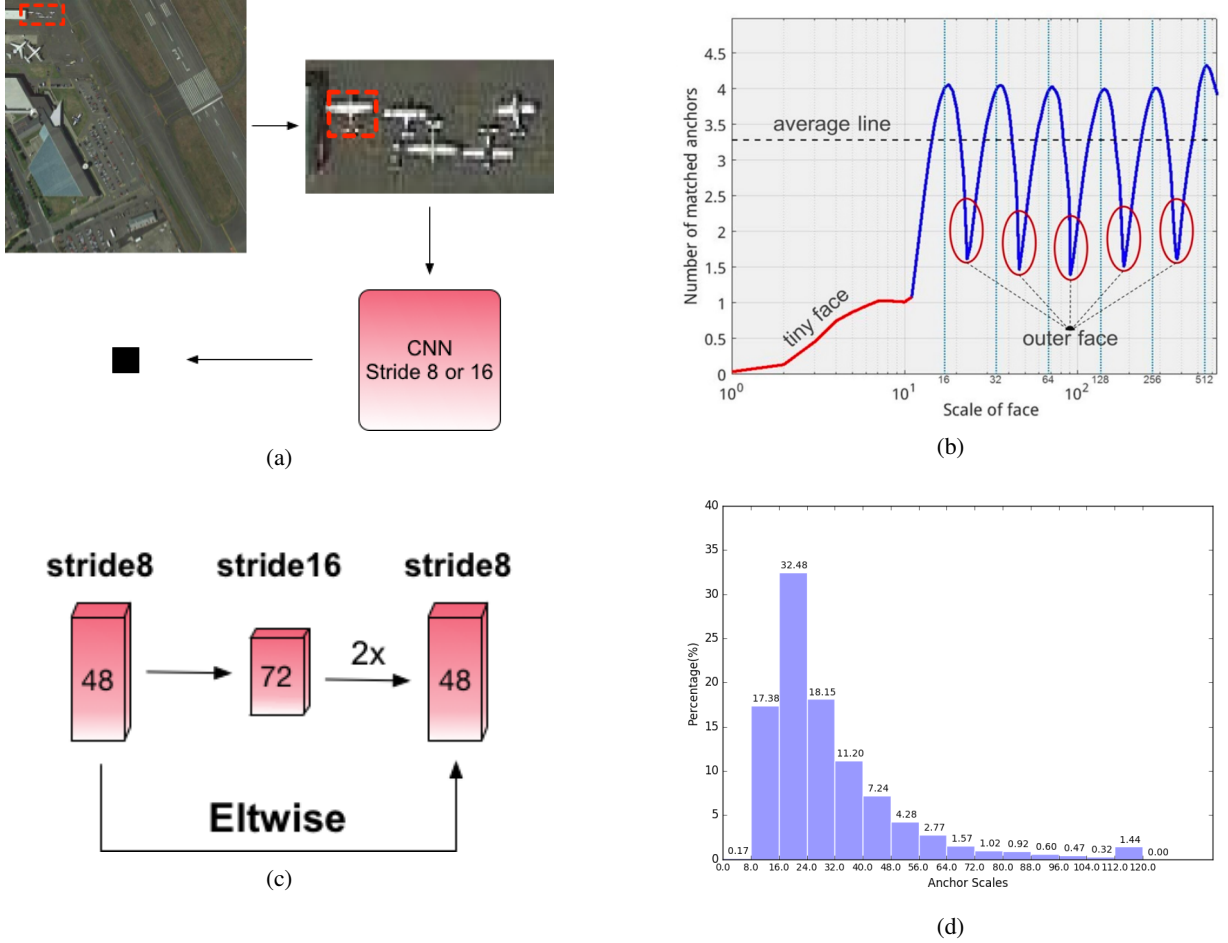


Fig. 4: (a) Few Features: Small objects have few features at detection layer. (b) Anchor matching analysis: the figure is from S^3FD [26], tiny and outer objects match too little anchors. (c) Our skip-connection architecture for reducing the anchor stride by enlarging the feature map. (d) Data Distribution: The bounding box scales of our training dataset.

ResNets. Thanks to this lightweight architecture, Tiny-Net can be trained from scratch and converge well just with a cycle training schedule, which iteratively update the step learning rate twice or more. Under this condition, Tiny-Net will not be influenced by the domain gap between natural images and remote sensing images.

Benefit from those characters, Tiny-Net can reduce inference cost and preserve powerful features for tiny object detection in remote sensing images, which further improved the efficiency of \mathcal{R}^2 -CNN.

C. Global Attention

Thanks to the unified classifier and detector, numerous blank patches are filtered by classifier, making false positives reduce obviously. But the problem still exists because of limited receptive field. When you see two similar objects, you can't distinguish what they are without context information. For example, when you see the top image in Fig 3-(a), you may confuse in this question: What exactly are they? But when you see two images below, you can easily distinguish them out. As discussed in [39], CNN has two types of receptive fields:

TABLE I: Architecture of our Tiny-Net. Each 3×3 block are residual block in ResNet [6] except conv-1.

layer name	output size	architecture
conv-1	640×640	$[3 \times 3, 12] \times 2$
conv-2	320×320	$\begin{bmatrix} 3 \times 3, 18 \\ 3 \times 3, 18 \end{bmatrix} \times 2$
conv-3	160×160	$\begin{bmatrix} 3 \times 3, 36 \\ 3 \times 3, 36 \end{bmatrix} \times 2$
conv-4	80×80	$\begin{bmatrix} 3 \times 3, 48 \\ 3 \times 3, 48 \end{bmatrix} \times 3$
conv-5	40×40	$\begin{bmatrix} 3 \times 3, 72 \\ 3 \times 3, 72 \end{bmatrix} \times 2$

the theoretical receptive field and the effective receptive field. Theoretical receptive field indicates the input region that can affect the value of this unit theoretically. However, not every pixel in the theoretical receptive field contributes equally to the final output. Only a subset of the area has effective influ-

ence on the output value, which is called effective receptive field. The effective receptive field is smaller than theoretical receptive field, as shown in Fig 3-(b). The limited effective receptive field leads the final feature map obtain few context information, thus leading to more false positives.

Inspired by this phenomenon, we use feature pyramid pooling as a global attention block on the top of Tiny-Net. The architecture is shown in Fig 3-(c). The feature maps are firstly pooled in different pyramid levels, such as 1×1 , 2×2 , and 4×4 . Then we recover the pooled features to their original scale with bilinear interpolation. The feature maps are fused additionally next. Feature maps can get more context information, and the receptive field will be also enlarged to the whole image. The global attention module fuses features from different pyramid scales, leads the detector pay more attention to the whole image. The detector is more discriminative with the help of more context information. We can found the confidence of false positives drop obviously with this module, as shown in Fig 3-(d), proving its effectiveness.

D. Detector

Our \mathcal{R}^2 -CNN is strong to detect tiny objects. The architecture of detection branch is shown in Fig 2-(c). State-of-art object detectors are mainly based on region proposal network in [7] framework, which use anchors to generate object proposals. Anchors are a set of pre-defined boxes with multiple scales and aspect ratios tiled regularly on the image plane. But anchor-based detectors drop performance drastically on objects with tiny sizes, such as less than 16×16 pixels, and those tiny objects are majority in remote sensing images, such as airplanes, ships, cars, etc. To tackle this problem, we first investigate why this is the case, and proposed a scale-invariant anchor strategy to tile anchors reasonably especially for small objects. On the other hand, we insert an efficient zoom-out and zoom-in architecture in Tiny-Net to enlarge the feature map without margin cost, which improve the recall of tiny objects obviously. Position sensitive RoI pooling is also used to get more spatial information. Through these ways, we get excellent results on tiny object detection.

1) **Why this is the case?:** Like in Fig 4-(a), the stride size of the lowest anchor-associated layer is too large (e.g. 16 pixels or 32 pixels), and the features losses along with the downsampling of pooling layer. Therefore tiny objects have been highly squeezed on these layers and have few features for detection. An airplane may be only 1×1 pixels in final feature map. On the other hand, the anchor scales are discrete (i.e., 16, 32, 64, $\dots 2^k$), but object scales are continuous. During training, an anchor will be assigned to a ground-truth box if its IoU with this box is the highest than other anchors, or its IoU is higher than a threshold T_h . When the object's scale is near to anchor scales, they will be attached more anchors, thus easier to be located. The face detector S^3 FD [26] which use SSD [24] architecture explained this phenomenon appropriately, we inference their statistics in Fig 4-(b). It shows the number of matched anchors at different face scales under 16, 32, 64, $\dots 2^k$ anchor scales. If an object has a scale over average line, it will be matched enough anchors. But tiny objects are matched little anchors, leading to performance drop drastically.

2) **Our Method:** To tile anchors more reasonably, we analyze bounding boxes' scale distribution of our training dataset, which is shown in Fig 4-(d). We can see tiny objects are majority in it. Instead of choosing anchors by hand, we run k-means clustering on the training set to automatically find good priors. Our training set's bounding box scales are $X : (x_1, x_2, \dots, x_n)$. There are k anchor scales we want, and the center scales are $(\mu_1, \mu_2, \dots, \mu_k)$. Scales are clustered in (s_1, s_2, \dots, s_k) . Through minimize:

$$\underset{i=1}{\operatorname{argmin}} \sum_{i=1}^k \sum_{x \in s_i} \|x - \mu_i\|^2, \quad (2)$$

we can get the clustered anchor scales.

To extract beneficial features for tiny object detection, one way is reducing the anchor stride by enlarging the feature map using a zoom-out and zoom-in architecture. Like shown in Fig 4-(c), we first zoom-out the feature map with a residual block, thus its anchor-stride is 16 pixels. Then a is employed to recover the feature maps are recovered to their original scale using a zoom-in operator. In addition, we use a skip-connection between stride-8 layer and the upsampled layer. We found the stride-16 layer can extract more high-level features, which are beneficial to object detection. And the skip-connection can fuse low-level features and high-level features, making final feature maps more discriminative.

Considering of the complicated backgrounds of remote sensing images, we use position-sensitive RoI pooling [8] in our detector instead of RoI pooling. RoI pooling apply a costly per-region subnetwork hundreds of times. If there are 1000 proposals, the detector will be tested 1000 times wastefully. In contrast to this operator, position-sensitive RoI pooling is fully convolutional with almost all computation shared on the entire image. Much computation is saved with this operator. On the other hand, position sensitive RoI pooling can address the dilemma between translation-invariance in image classification and translation-variance in object detection. More spatial information are extracted, thus leading to better performance.

IV. EXPERIMENTS

In this section, we first present the implementations of our \mathcal{R}^2 -CNN, such as datasets, evaluation metric and parameter settings. The results of our network and comparative experiments are then discussed.

A. Implementations

1) **Datasets:** Due to the lack of standard datasets of large-scale remote sensing images, we collected 1169 GF-1 images and 318 GF-2 images, which are 18000×18192 pixels, 2.0m resolution and 27620×29200 pixels, 0.8m resolution respectively. In addition, we collected 38472 pieces of 640×640 images which contain target objects from the publicly available Google Earth service to supplement the poor positive patches in GF images. All images are cropped in patches of 640×640 pixels with 20% overlap. In particularly, if we have a maximum object scale d , and a cropped scale D , we recommend an overlap $\frac{d}{D}$. For example, as the scales in Fig.4-(d), the

TABLE II: \mathcal{R}^2 -CNN's results in *GF1-test-dev*, results are shown in unified / un-unified / fully detection training and testing.

Score Thre	TP	FP	Recall	Precision
0.05	613 / 593 / 616	186 / 264 / 8126	99.35 / 96.11 / 99.84	76.72 / 69.19 / 6.97
0.5	607 / 591 / 612	46 / 93 / 561	98.38 / 95.79 / 99.19	92.96 / 86.40 / 52.17
0.8	593 / 577 / 596	15 / 41 / 264	96.11 / 93.52 / 96.60	97.53 / 93.36 / 69.30
0.85	591 / 573 / 592	10 / 29 / 189	95.78 / 92.87 / 95.95	98.33 / 95.18 / 75.80
0.9	579 / 568 / 586	7 / 18 / 131	93.84 / 92.06 / 94.98	98.80 / 96.93 / 81.73
0.95	556 / 542 / 561	3 / 7 / 37	90.11 / 87.84 / 90.92	99.46 / 98730 / 93.81

TABLE III: \mathcal{R}^2 -CNN's results in *GF2-test-dev*, results are shown in unified / un-unified / fully detection training and testing.

Score Thre	TP	FP	Recall	Precision
0.05	108 / 79 / 113	74 / 173 / 5746	93.91 / 68.69 / 98.26	59.34 / 31.35 / 1.93
0.5	107 / 77 / 111	14 / 34 / 217	93.04 / 66.95 / 96.52	88.43 / 69.36 / 33.84
0.8	105 / 74 / 108	8 / 21 / 69	91.30 / 64.34 / 93.91	92.92 / 77.89 / 61.01
0.85	104 / 74 / 106	5 / 17 / 47	90.43 / 64.34 / 92.17	95.41 / 81.32 / 69.28
0.9	100 / 72 / 105	2 / 13 / 31	86.96 / 62.60 / 91.30	98.04 / 84.71 / 77.20
0.95	96 / 69 / 100	1 / 7 / 13	83.48 / 60.00 / 86.96	98.97 / 90.79 / 88.49

maximum scale of the objects in our dataset is about 128, the cropped scale is 640, thus a 20% overlap is applied to not only prevent the object from being truncated off but also augment the datasets. To help the converge of the network, we control the proportion of positive patches and negative patches to be 1 : 3 to obtain a balanced training set. The negative patches are selected using hard example boosting to enhance the training process.

We collect 102 GF-1 images as *GF1-test-dev* and 40 GF-2 images as *GF2-test-dev* to evaluate the ability of \mathcal{R}^2 -CNN. To evaluate our model more exhaustively, we collected 4633 images (640×640 pixels) from Google Earth as *Rgb-test-dev* and 1000 images (640×640 pixels) from GF-1 and GF-2 as *Gray-test-dev*, which help us evaluate the ability of the detector.

2) **Evaluation Metric:** Considering of the few target objects in large-scale remote sensing images and the requirement for practical engineering applications, we evaluation our \mathcal{R}^2 -CNN with *Recall* and *Precision* of different score thresholds. The correct number of detections is true positives *TP*, and the number of spurious detections of the same object is false positives *FP*. The number of ground-truth instances is *NP*. The precision and recall following:

$$Precision = \frac{TP}{TP + FP}, \quad (3)$$

$$Recall = \frac{TP}{NP}, \quad (4)$$

We also show the instance number in details for more intuitional and convincing. Considering of numerous negative scene of classifier, the *Accuracy* are generally over 99.0%, making this metric meaningless. So we use *Recall*, *Precision* and instance number to evaluate our classifier. We use *mAP*

and *Max-Recall* with a score threshold of 0.05 as in PASCAL-VOC [40] to evaluate our detector, which are defined as:

$$mAP = \frac{1}{Q} \sum_{q=1}^Q AP(q), \quad (5)$$

$$AP = \frac{\sum_{k=1}^n (P(k) \times r(k))}{|R(q)|}, \quad (6)$$

where Q is the number of categories, $|R(q)|$ is the number of images relevant to the category q , k is the rank in the sequence of retrieved images, and n is the total number of retrieved images. $P(k)$ is the precision at cutoff k in the list, and $r(k)$ is an indicator function whose value is 1 if the image at rank k is relevant and is 0 otherwise.

3) **Parameter Settings:** We adopt synchronized SGD training on 8 GPUs with synchronized batch normalization. A mini-batch involves 1 image per GPU and 512 proposals per image for detector training. We use a momentum of 0.9 and a weight decay of 0.0005. We use a learning rate of 0.001 for 80k mini-batches, and 0.0001, 0.00001 for the next 80k and 40k mini-batches. The learning rate and training epochs are iterated twice as a cycle schedule because of the network is trained from scratch. We randomly initialize all layers by drawing weights from a zero-mean Gaussian distribution with standard deviation 0.01. The anchor's scales in RPN we used in our final model is [1, 2, 4, 10, 16, 30] with a stride of 8, and the anchor's ratio is 1 considering of airplane's shape. Other implementation details are as in [6] and [7]. We also use multi-scale training with scale [513, 609, 721, 801, 913], and online hard example mining [29] for hard example boosting. We stretch remote sensing images from uint16 to uint8 by divided a factor of 4. We also stretch the images' histogram with a factor in [0, 0.02], which can not only inhibit the noise in remote sensing images, but also as a data augmentation method. We augment the data online with rotate and flip randomly. Our implementation use Caffe [41].

TABLE IV: Results of classifier on *GF1-test-dev*. \vdash means fine-tuning from ImageNet pre-trained model. \dashv means training from scratch. $-$ means training without detector.

Model	TP	FP	Recall	Precision	Time Cost
ResNet-50 \vdash $-$ [6]	134	34	87.01	79.76	48.21 ms
ResNet-50 \dashv $-$ [6]	128	29	83.12	81.53	48.21 ms
Ours $-$	105	179	68.18	36.97	16.63 ms
\mathcal{R}^2 -CNN	148	45	96.10	76.68	16.63 ms

TABLE V: Results of classifier on *GF2-test-dev*. \vdash means fine-tuning from ImageNet pre-trained model. \dashv means training from scratch. $-$ means training without detector.

Model	TP	FP	Recall	Precision	Time Cost
ResNet-50 \vdash $-$ [6]	61	2	68.54	96.83	48.21 ms
ResNet-50 \dashv $-$ [6]	82	204	92.13	28.67	48.21 ms
Ours $-$	55	67	61.80	43.65	16.63 ms
\mathcal{R}^2 -CNN	82	38	92.13	68.33	16.63 ms

B. Evaluation of \mathcal{R}^2 -CNN

We comprehensively evaluate our method on the *GF1-test-dev* and *GF2-test-dev*. The results are shown in Table II and Table III. It is **efficient**, we can process a 18000×18192 GF-1 image in 29.4s on Titian X just with single thread. It is **robust**, with a score threshold of 0.85, there are only 10 false positives in *GF1-test-dev* and 5 false positives in *GF2-test-dev*. It is **strong**, we can get 95.78 *Recall* and 98.33 *Precision* on *GF1-test-dev* also with a score threshold of 0.85, showing its potential from practical application. We compared our \mathcal{R}^2 -CNN with un-unified (train and test separately) network and fully detection network. Results show when we joint detector with classifier, they can promote each other to get the best results. When the network is un-unified, the classifier can't obtain enough discrimination without the feature extracted by detector, leading *Recall* and *Precision* drop obviously. When detecting the objects all using detector, too many false positives appeared and the efficiency is lower considering of the heavy detector. Our network achieves a superior results on performance and speed, showing its **efficient**, **robust**, and **strong**.

1) **Efficient**: Tiny-Net enables the inference time of network more less than ResNet-50 or other large models and preserve powerful features for object detection, details are shown in Table IV and Table V. The classifier with Tiny-Net costs 16.63 ms with 640×640 inputs on Titian X, and the detector costs 45.21 ms with the same setting. The detector is three times slower than classifier. In our *GF1-test-dev*, there are only 154 patches have target objects. The unified architecture make 99.9% of the total patches do not need to pass the heavy detector branch. Total costs of our network and fully detection network is shown in Table VI. We can process a 18000×18192 GF-1 image in 29.4s on Titian X just with single thread. Though there is still a long way to build a real-time detection system on large-scale remote sensing

TABLE VI: Time costs of different methods with single thread.

Benchmark	\mathcal{R}^2 -CNN	Detection
<i>GF1-test-dev</i>	29.4 s	64.7 s
<i>GF2-test-dev</i>	66.2 s	163.7 s

TABLE VII: Performance with or without global attention block.

Score Thre	TP	FP	Recall	Precision
0.05	613 / 611	186 / 216	99.35 / 99.03	76.72 / 73.88
0.5	607 / 609	46 / 101	98.38 / 98.70	92.96 / 85.77
0.8	593 / 600	15 / 63	96.11 / 97.24	97.53 / 90.49
0.85	591 / 597	10 / 49	95.78 / 96.76	98.33 / 92.41
0.9	579 / 582	7 / 27	93.84 / 94.33	98.80 / 95.56
0.95	556 / 559	3 / 11	90.11 / 90.60	99.46 / 98.07

images, our network tackle the problem well with the proposed methods.

2) **Robust**: The unified classifier can identify the difficult situation even when there is only one tiny objects in the patch given the fine-grained feature extracted by detector, and the detector receives less false positive candidates since most of them are filtered out by classifier. Results are shown in Table IV and Table V. Because of the large memory needed by ResNet-50 with an anchor-stride of 8, we can't evaluate our \mathcal{R}^2 -CNN with ResNet-50. Thus the setting of ResNet-50 are same as [6] without detector. *GF1-test-dev* is cropped in 131148 patches with 640×640 pixels and 20% overlap, and there are also 123120 patches from *GF2-test-dev*. The *Recall* and *Precision* only consider the positive patches. Results of our \mathcal{R}^2 -CNN get the best results compared to others. Classifier drop performance drastically without detector, and the recall of our \mathcal{R}^2 -CNN is higher than ResNet-50, showing the effectiveness of the features extracted by detector. Though there are more false positives in our model, the detector can rectify the results later. We have attempted to train ResNet-50 from scratch to break the domain gap within natural images and remote sensing images, but get bad results. We argue that is mainly because the numerous parameters of ResNet-50 but the small amount of training sets. Though there are hundreds of thousands remote sensing images for us, only little of them can be use during training time to handle the positive-negative imbalance problem.

Besides, we evaluate the effectiveness of global attention block on *GF1-test-dev*. Results are shown in Table VII. When \mathcal{R}^2 -CNN is implemented without global attention block, there are more false positives because of the limited receptive field. With global attention block, the confidence of false positives drop obviously. We found the recall drop a little with global attention block. But comparing to the enhancement of inhibiting false positives, that is a better model for practical engineering.

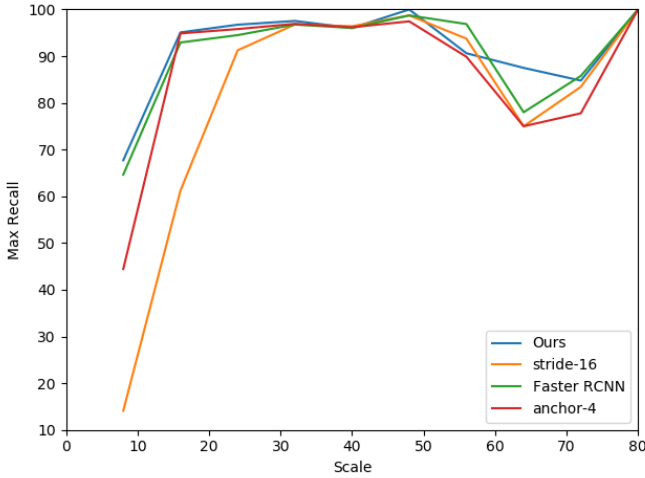
3) **Strong**: To validate the effectiveness of \mathcal{R}^2 -CNN on tiny object detection, we evaluate our network on *Rgb-test-dev* and *Gray-test-dev*. Results are shown in Table VIII and Table IX.

TABLE VIII: Results of detectors on *Rgb-test-dev*. - means training without classifier. + means training with ImageNet pre-trained model.

Metric	stride-16	No Conv-5	ResNet-50 ⁺ [8]	Faster R-CNN [7]	Anchor-4	Anchor-5	Anchor-8	Ours ⁻	\mathcal{R}^2 -CNN
mAP (%)	84.73	93.74	83.86	94.61	94.95	95.12	96.43	95.81	96.04
Max Recall (%)	87.21	95.40	86.34	95.62	96.38	96.74	97.88	97.12	97.26
Time cost (ms)	31.93	41.81	58.26	49.26	39.58	42.53	50.07	45.21	45.21

TABLE IX: Results of detectors on *Gray-test-dev*. - means training without classifier. + means training with ImageNet pre-trained model.

Metric	stride-16	No Conv-5	ResNet-50 ⁺ [8]	Faster R-CNN [7]	Anchor-4	Anchor-5	Anchor-8	Ours ⁻	\mathcal{R}^2 -CNN
mAP (%)	83.68	95.16	82.53	94.90	94.56	95.35	97.47	97.01	97.25
Max Recall (%)	85.19	96.15	84.07	96.04	95.58	96.49	98.23	98.13	98.03
Time cost (ms)	31.93	41.81	58.26	49.26	39.58	42.53	50.07	45.21	45.21

Fig. 5: Max-Recall of different scales in *Gray-test-dev*.

How important is the zoom-out and zoom-in architecture?

Considering of the large memory needed by ResNet-50 with an anchor-stride of 8 pixels, detector with ResNet-50 is implemented with an anchor-stride of 16 pixels. The results of *stride-16* with \mathcal{R}^2 -CNN only get 83.68 mAP in *Gray-test-dev*. Besides, the mAP of different scales are shown in Fig 5. The performance of objects larger than 32 pixels is basically comparable to our method, but the results of small objects drop obviously without the architecture. In additional, we attempt to attach the global attention block to *conv-4* directly. The results of *No Conv-5* drop 2 points compared to our method. This modification shows that *Conv-5* can extract more high-level features which are benefit for object detection, proving the effectiveness of this architecture.

How important is our anchor strategy? The number of clustered points is a hand-craft parameter in k-means. We attempt to cluster anchor scales with a number of 4, 5, 6 and 8. Results with different anchor scales are shown below:

4 anchor scales: [2.87, 5.44, 11.39, 26.72]

5 anchor scales: [2.32, 4.51, 7.62, 13.57, 28.34]

TABLE X: Comparison experiments with FPN Faster R-CNN and Mask R-CNN on *rgb-test-dev*. - means training without classifier.

Metric	mAP (%)	Max Recall (%)
FPN Faster RCNN	96.07	96.55
Mask R-CNN	96.20	96.63
FPN Faster R-CNN with Tiny-Net	95.37	96.28
Ours ⁻	95.81	96.04
\mathcal{R}^2 -CNN	96.04	97.26

6 anchor scales: [2.18, 3.90, 6.17, 9.8, 15.91, 29.83]

8 anchor scales: [1.97, 3.14, 4.8, 7.05, 10.53, 15.52, 24.55]

Max-Recall of different scales are shown in Table VIII and Table IX. Results show that the distribution of anchors can better fit the dataset to reach better performance with this strategy. We found *Anchor-6* get an excellent trade-off between efficiency and performance, so that's the final parameter of our \mathcal{R}^2 -CNN.

How important is position-sensitive RoI pooling? Compared with Faster R-CNN [7], our \mathcal{R}^2 -CNN improves mAP by 2.35 points in *Gray-test-dev*, particularly in tiny objects. The spatial information is better encoded via position-sensitive RoI pooling, which is beneficial for tiny object detection. Moreover, the time costs is 49.26 ms for Faster R-CNN but 45.21ms for \mathcal{R}^2 -CNN with position-sensitive RoI pooling. Through sharing all proposals' weights, we instead recalculating the feature maps of all proposals of voting from the final feature maps. This modification is also greatly helpful for efficient process especially when there are numerous patches.

Comparison experiments with state-of-the-art. To validate the effectiveness of our architecture, comparison experiments are implemented with FPN Faster R-CNN and Mask R-CNN. Considering the lack of mask annotations, Mask R-CNN is only implemented with RoI Align. Both methods are implemented with a ResNet-50 backbone. Results are shown in Table X. The comparable results prove the effectiveness of \mathcal{R}^2 -CNN. We also found that the RoI Align brings little

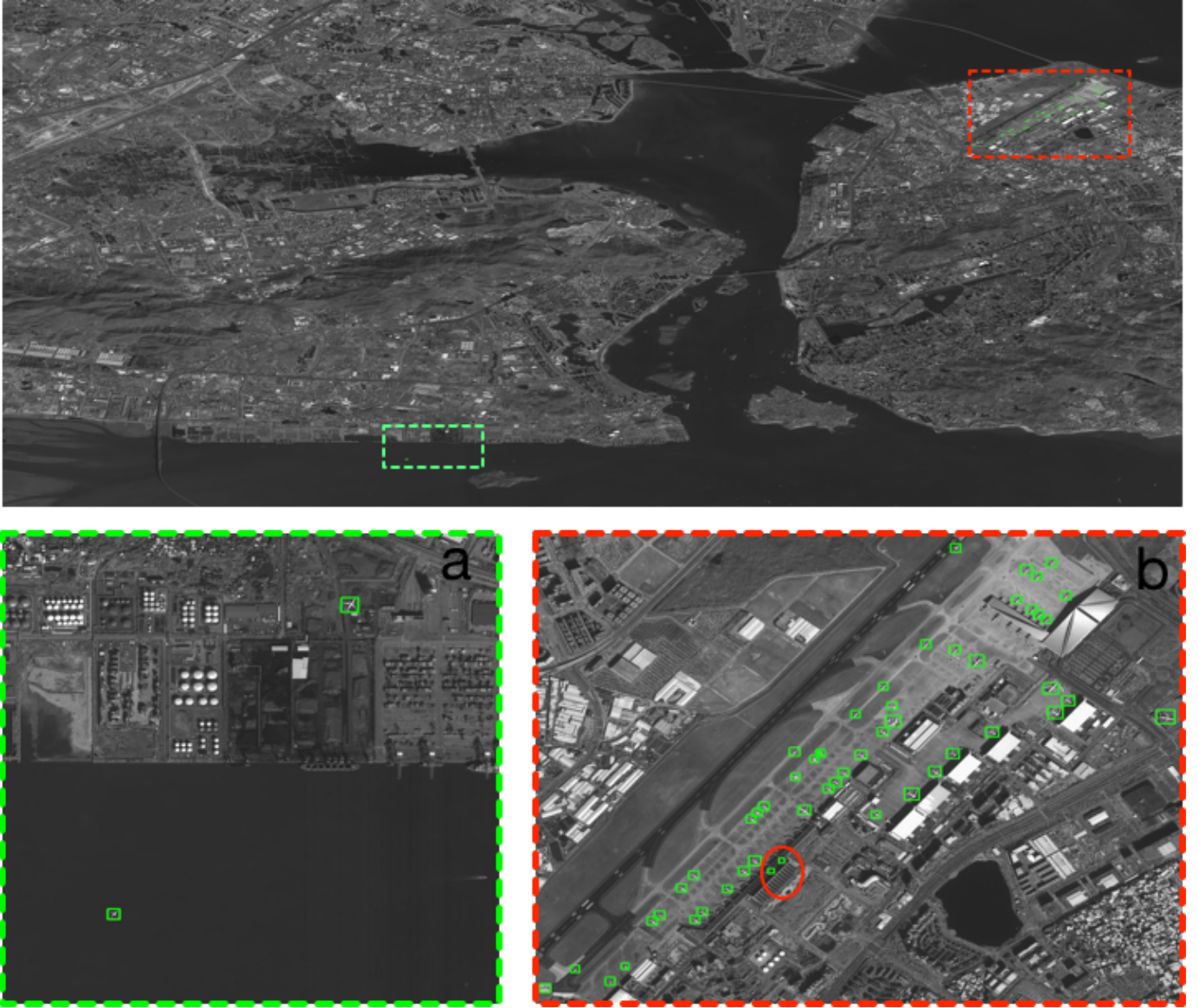


Fig. 6: Results of our \mathcal{R}^2 -CNN with a score threshold of 0.9. Two airplanes are flying back to airport in image-a. Results of the airport is shown in image-b. Two objects marked by the red circle in image-b are false positives.

improvement to the FPN Faster R-CNN baseline. Considering the tiny objects are dominating our dataset, this result is reasonable because of the potential of RoI Align is not fully explored because of the small feature maps. The result of FPN Faster R-CNN with Tiny-Net is 0.5 points lower than \mathcal{R}^2 -CNN training without classifier reinforced, proving the effectiveness of the specific design for Tiny-Net. All those results show that our \mathcal{R}^2 -CNN reach a great trade-off within efficient processing, false positives inhibiting and tiny object detection.

C. Discussion

In our experiments, we get a pretty surprising results in Fig 7. That is an image under heavy haze. We found we can detect the aircrafts easily. The confidence of those objects are higher than 0.9, but lower than 0.95. It is not a high

score in our results (a high confidence is larger than 0.99), but still enough for practical engineering applications. We must recognize this gratifying results are not only coming from the reasonable architecture of our \mathcal{R}^2 -CNN, but also the precise annotation of similar situations in our training set. The backbone, classifier and detector are specially designed to converge well while training from scratch. That's a meaningful results for us to understand the powerful generalization ability of Deep Convolutional Neural Networks. However, annotating all those terrible conditions very well is not a sensible selection. But we can still explore why this is the case and how does CNN execute such well, to push the meaningful research in those situations. There are numerous remote sensing resources to utilize and problems to solve. With more and more powerful operators and theories, we hope we can fast promote the development of real-time remote sensing

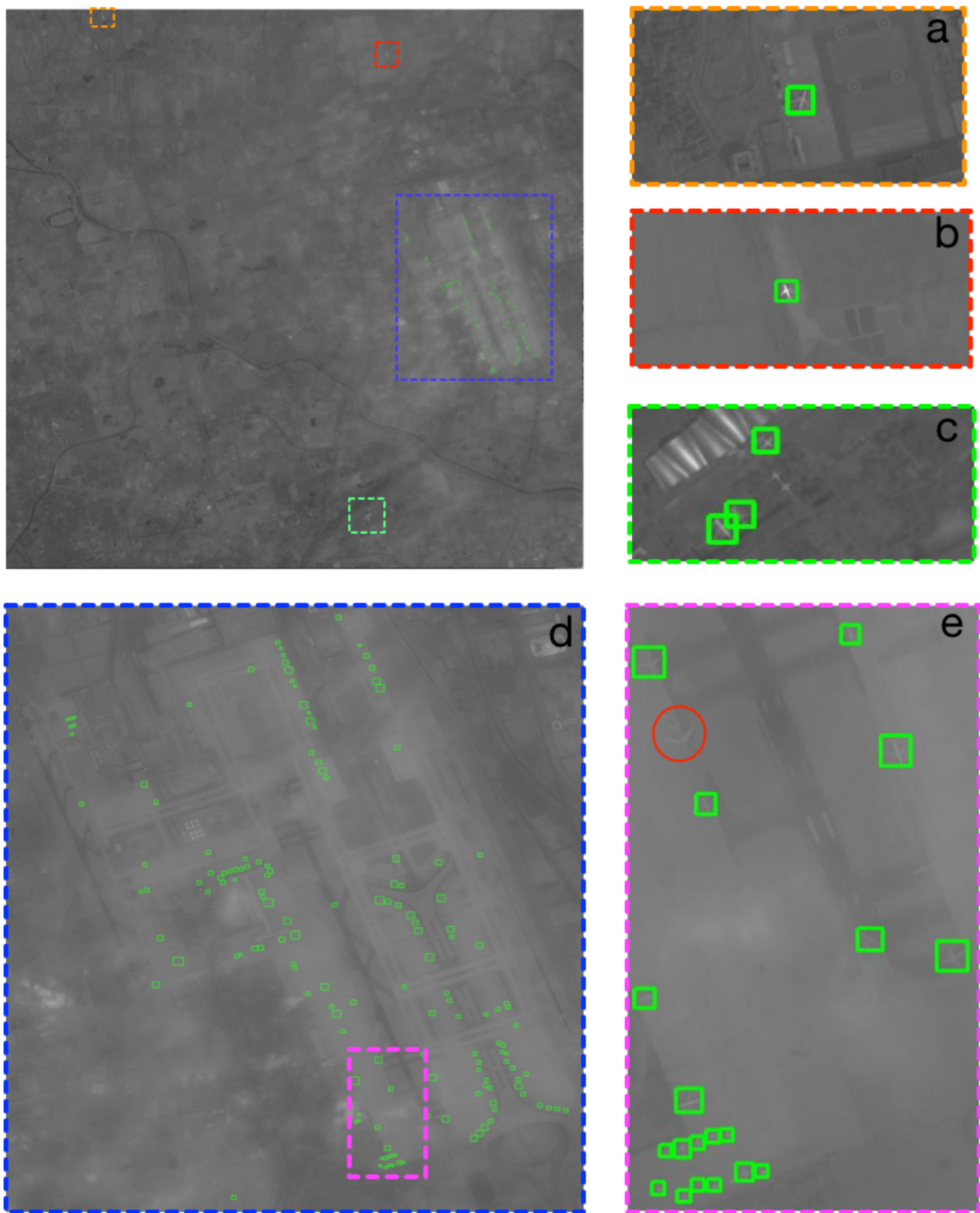


Fig. 7: Results of our \mathcal{R}^2 -CNN with a score threshold of 0.9. The area is under heavy haze. Image-a shows an airplane in the wild. Image-b shows a airplane flying in sky. Image-c shows an airport with some airplanes. Image-d shows the results of airport. Image-e shows the details of d. The ignored airplane marked by red circle in image-e has a confidence of 0.83.

systems in the future.

V. CONCLUSION

We proposed \mathcal{R}^2 -CNN, a unified and self-reinforced convolutional neural network under the end-to-end training framework, which joint the classifier and detector elegantly. The lightweight backbone Tiny-Net extracts powerful features from inputs quickly, and the intermediate global attention block enlarge the receptive field to inhibit false positives. The classifier first predict the existence of detection target in current patch, and the specifically designed detector is followed to locate them accurately if available. The high recall and precision in GF-1 and GF-2 validate the effectiveness of our network. Specifically, we can process a GF-1 image in 29.4s on Titian X just with single thread. All those experiments prove our \mathcal{R}^2 -CNN is *efficient* in both computation and memory consumption, *robust* to false positives and *strong* to detect tiny objects.

REFERENCES

- [1] J. Han, D. Zhang, G. Cheng, L. Guo, and J. Ren, "Object detection in optical remote sensing images based on weakly supervised learning and high-level feature learning," *IEEE Transactions on Geoscience and Remote Sensing*, vol. 53, no. 6, pp. 3325–3337, 2015. 1, 3
- [2] Y. Long, Y. Gong, Z. Xiao, and Q. Liu, "Accurate object localization in remote sensing images based on convolutional neural networks," *IEEE Transactions on Geoscience and Remote Sensing*, vol. 55, no. 5, pp. 2486–2498, 2017. 1, 3
- [3] X. Bai, H. Zhang, and J. Zhou, "Vhr object detection based on structural feature extraction and query expansion," *IEEE Transactions on Geoscience and Remote Sensing*, vol. 52, no. 10, pp. 6508–6520, 2014. 1, 3
- [4] F. Zhang, B. Du, L. Zhang, and M. Xu, "Weakly supervised learning based on coupled convolutional neural networks for aircraft detection," *IEEE Transactions on Geoscience and Remote Sensing*, vol. 54, no. 9, pp. 5553–5563, 2016. 1, 3
- [5] Z. Lei, T. Fang, H. Huo, and D. Li, "Rotation-invariant object detection of remotely sensed images based on texon forest and hough voting," *IEEE Transactions on Geoscience and Remote Sensing*, vol. 50, no. 4, pp. 1206–1217, 2012. 1, 3
- [6] K. He, X. Zhang, S. Ren, and J. Sun, "Deep residual learning for image recognition," in *Proceedings of the IEEE conference on computer vision and pattern recognition*, 2016, pp. 770–778. 2, 4, 5, 7, 8
- [7] S. Ren, K. He, R. Girshick, and J. Sun, "Faster r-cnn: Towards real-time object detection with region proposal networks," in *Advances in neural information processing systems*, 2015, pp. 91–99. 2, 4, 6, 7, 9
- [8] J. Dai, Y. Li, K. He, and J. Sun, "R-fcn: Object detection via region-based fully convolutional networks," in *Advances in neural information processing systems*, 2016, pp. 379–387. 2, 6, 9
- [9] D. G. Lowe, "Distinctive image features from scale-invariant keypoints," *International journal of computer vision*, vol. 60, no. 2, pp. 91–110, 2004. 2
- [10] G. Tsai, "Histogram of oriented gradients," *University of Michigan*, vol. 1, no. 1, pp. 1–17, 2010. 2
- [11] Z. Xiao, Q. Liu, G. Tang, and X. Zhai, "Elliptic fourier transformation-based histograms of oriented gradients for rotationally invariant object detection in remote-sensing images," *International Journal of Remote Sensing*, vol. 36, no. 2, pp. 618–644, 2015. 2
- [12] G. Cheng and J. Han, "A survey on object detection in optical remote sensing images," *ISPRS Journal of Photogrammetry and Remote Sensing*, vol. 117, pp. 11–28, 2016. 2
- [13] Y. LeCun, L. Bottou, Y. Bengio, and P. Haffner, "Gradient-based learning applied to document recognition," *Proceedings of the IEEE*, vol. 86, no. 11, pp. 2278–2324, 1998. 2
- [14] A. Krizhevsky, I. Sutskever, and G. E. Hinton, "Imagenet classification with deep convolutional neural networks," in *Advances in neural information processing systems*, 2012, pp. 1097–1105. 2
- [15] M. Lin, Q. Chen, and S. Yan, "Network in network," *arXiv preprint arXiv:1312.4400*, 2013. 2
- [16] K. Simonyan and A. Zisserman, "Very deep convolutional networks for large-scale image recognition," *arXiv preprint arXiv:1409.1556*, 2014. 2, 4
- [17] C. Szegedy, W. Liu, Y. Jia, P. Sermanet, S. Reed, D. Anguelov, D. Erhan, V. Vanhoucke, A. Rabinovich *et al.*, "Going deeper with convolutions," *Cvpr*, 2015. 2
- [18] P. Sermanet, D. Eigen, X. Zhang, M. Mathieu, R. Fergus, and Y. LeCun, "Overfeat: Integrated recognition, localization and detection using convolutional networks," *arXiv preprint arXiv:1312.6229*, 2013. 2
- [19] R. Girshick, J. Donahue, T. Darrell, and J. Malik, "Rich feature hierarchies for accurate object detection and semantic segmentation," in *Proceedings of the IEEE conference on computer vision and pattern recognition*, 2014, pp. 580–587. 2, 4
- [20] J. R. Uijlings, K. E. Van De Sande, T. Gevers, and A. W. Smeulders, "Selective search for object recognition," *International journal of computer vision*, vol. 104, no. 2, pp. 154–171, 2013. 2
- [21] K. He, X. Zhang, S. Ren, and J. Sun, "Spatial pyramid pooling in deep convolutional networks for visual recognition," in *European conference on computer vision*. Springer, 2014, pp. 346–361. 2
- [22] R. Girshick, "Fast r-cnn," *arXiv preprint arXiv:1504.08083*, 2015. 2
- [23] J. Redmon, S. Divvala, R. Girshick, and A. Farhadi, "You only look once: Unified, real-time object detection," in *Proceedings of the IEEE conference on computer vision and pattern recognition*, 2016, pp. 779–788. 2
- [24] W. Liu, D. Anguelov, D. Erhan, C. Szegedy, S. Reed, C.-Y. Fu, and A. C. Berg, "Ssd: Single shot multibox detector," in *European conference on computer vision*. Springer, 2016, pp. 21–37. 2, 6
- [25] T.-Y. Lin, P. Dollár, R. B. Girshick, K. He, B. Hariharan, and S. J. Belongie, "Feature pyramid networks for object detection," in *CVPR*, vol. 1, no. 2, 2017, p. 3. 2
- [26] S. Zhang, X. Zhu, Z. Lei, H. Shi, X. Wang, and S. Z. Li, "S3fd: Single shot scale-invariant face detector," *arXiv preprint arXiv:1708.05237*, 2017. 2, 5, 6
- [27] P. Hu and D. Ramanan, "Finding tiny faces," in *Computer Vision and Pattern Recognition (CVPR), 2017 IEEE Conference on*. IEEE, 2017, pp. 1522–1530. 2
- [28] H. Zhao, J. Shi, X. Qi, X. Wang, and J. Jia, "Pyramid scene parsing network," in *IEEE Conf. on Computer Vision and Pattern Recognition (CVPR)*, 2017, pp. 2881–2890. 2
- [29] A. Shrivastava, A. Gupta, and R. Girshick, "Training region-based object detectors with online hard example mining," in *Proceedings of the IEEE Conference on Computer Vision and Pattern Recognition*, 2016, pp. 761–769. 3, 7
- [30] F. Hu, G.-S. Xia, J. Hu, and L. Zhang, "Transferring deep convolutional neural networks for the scene classification of high-resolution remote sensing imagery," *Remote Sensing*, vol. 7, no. 11, pp. 14 680–14 707, 2015. 3
- [31] L. Zhang, Z. Shi, and J. Wu, "A hierarchical oil tank detector with deep surrounding features for high-resolution optical satellite imagery," *IEEE Journal of Selected Topics in Applied Earth Observations and Remote Sensing*, vol. 8, no. 10, pp. 4895–4909, 2015. 3
- [32] T. Ishii, R. Nakamura, H. Nakada, Y. Mochizuki, and H. Ishikawa, "Surface object recognition with cnn and svm in landsat 8 images," in *Machine Vision Applications (MVA), 2015 14th IAPR International Conference on*. IEEE, 2015, pp. 341–344. 3
- [33] I. Ševo and A. Avramović, "Convolutional neural network based automatic object detection on aerial images," *IEEE geoscience and remote sensing letters*, vol. 13, no. 5, pp. 740–744, 2016. 3
- [34] A.-B. Salberg, "Detection of seals in remote sensing images using features extracted from deep convolutional neural networks," in *Geoscience and Remote Sensing Symposium (IGARSS), 2015 IEEE International*. IEEE, 2015, pp. 1893–1896. 3
- [35] G. Cheng, P. Zhou, and J. Han, "Learning rotation-invariant convolutional neural networks for object detection in vhr optical remote sensing images," *IEEE Transactions on Geoscience and Remote Sensing*, vol. 54, no. 12, pp. 7405–7415, 2016. 3
- [36] H. Zhu, X. Chen, W. Dai, K. Fu, Q. Ye, and J. Jiao, "Orientation robust object detection in aerial images using deep convolutional neural network," in *Image Processing (ICIP), 2015 IEEE International Conference on*. IEEE, 2015, pp. 3735–3739. 3
- [37] Q. Jiang, L. Cao, M. Cheng, C. Wang, and J. Li, "Deep neural networks-based vehicle detection in satellite images," in *Bioelectronics and Bioinformatics (ISBB), 2015 International Symposium on*. IEEE, 2015, pp. 184–187. 3
- [38] J. Deng, W. Dong, R. Socher, L.-J. Li, K. Li, and L. Fei-Fei, "Imagenet: A large-scale hierarchical image database," in *Computer Vision and*

- Pattern Recognition, 2009. CVPR 2009. IEEE Conference on.* IEEE, 2009, pp. 248–255. 4
- [39] W. Luo, Y. Li, R. Urtasun, and R. Zemel, “Understanding the effective receptive field in deep convolutional neural networks,” in *Advances in Neural Information Processing Systems*, 2016, pp. 4898–4906. 5
- [40] M. Everingham, L. Van Gool, C. K. Williams, J. Winn, and A. Zisserman, “The pascal visual object classes (voc) challenge,” *International journal of computer vision*, vol. 88, no. 2, pp. 303–338, 2010. 7
- [41] Y. Jia, E. Shelhamer, J. Donahue, S. Karayev, J. Long, R. Girshick, S. Guadarrama, and T. Darrell, “Caffe: Convolutional architecture for fast feature embedding,” in *Proceedings of the 22nd ACM international conference on Multimedia.* ACM, 2014, pp. 675–678. 7